

2022-05-25

Beach Hazards: Riu Funana, Cape Verde v3b.

Stokes, C

<http://hdl.handle.net/10026.1/19265>

All content in PEARL is protected by copyright law. Author manuscripts are made available in accordance with publisher policies. Please cite only the published version using the details provided on the item record or document. In the absence of an open licence (e.g. Creative Commons), permissions for further reuse of content should be sought from the publisher or author.

BEACH HAZARDS: RIU FUNANA, CAPE VERDE



Report provided by: Coastal Marine Applied Research,
University of Plymouth Enterprise Ltd.

Report provided for: Adam Wooler

Date: 24/05/2022

Project code: 2109

Document code/version: 2109_v3b

**Coastal Marine
Applied Research**



A research-informed consultancy to address
important issues in the coastal and marine environment

CMAR: Coastal Marine Applied Research

CMAR is a research-informed consultancy group based in the School of Biological and Marine Sciences at the University of Plymouth, south west UK, and contract our services through the university's wholly owned commercial subsidiary, University of Plymouth Enterprise Limited (UoPEL). We focus on coastal processes and marine physics, and aim to provide a first-class data collection, analysis, modelling, and synthesis service to help address important issues in the coastal and marine environment. We strive to understand and predict the behaviour of coastal, marine and estuarine systems to support the appropriate management of resources and activities in these environments. Our team consists of highly qualified coastal scientists and engineers, and our research on coastal dynamics is published in international, peer-reviewed journals.

DISCLAIMER

Whilst UoPEL will use all reasonable endeavours to ensure the accuracy of the work performed and any information given, UoPEL makes no warranty, express or implied, as to accuracy and will not be held responsible for any consequence arising out of any inaccuracies or omissions unless such inaccuracies or omissions are the result of negligence on the part of UoPEL or its agents.

The obligations of UoPEL and its agents shall cease upon delivery of the report and no liability whatsoever either direct or indirect shall rest upon them for the effects of any product or process that may be produced or adopted by the client or any other party, notwithstanding that the formulation of such product or process may be based upon the findings of the report.

UoPEL shall not be liable for any death or injury unless it is caused by the negligence of UoPEL or its agents, nor shall it be liable for any loss or damage whatsoever unless it is caused by its wilful default or that of its agents.

All queries related to this document should be directed to:

CMAR, School of Biological and Marine Sciences, Reynolds Building, University of Plymouth,
Drake Circus, Plymouth, Devon PL4 8AA

Email: cmar@plymouth.ac.uk

Telephone: +44 1752 586177

Web: www.plymouth.ac.uk/cmar

Twitter: @pu_cmar

Document Information


Document permissions	Adam Wooler
Project number	2109
Project name	BEACH HAZARDS: RIU FUNANA, CAPE VERDE
Report date	24 th May 2022
Report number	2109_v3b
Client	Adam Wooler
Client representative	Adam Wooler
Project lead	Dr Christopher Stokes
Project manager	Prof. Gerd Masselink
Report Citation	CMAR, 2022. Beach Hazards: Riu Funana, Cape Verde. Report 2109_v3b, UPEL, 38 pp.

Document history

Date	Issue	Prepared	Approved	Authorised	notes
13/07/21	Draft	LB/CS	GM	GM	
15/12/21	Final	LB	GM	GM	
24/05/22	Final	LB/CS	GM	GM	Additional analysis

Document authorisation

Prepared



Dr Christopher Stokes

Approved



Prof. Gerd Masselink

Authorised



Prof. Gerd Masselink

Cape Verde Beach Hazards

Executive Summary

Coastal Marine Applied Research (CMAR) have been commissioned by Adam Wooler to assess physical bathing hazards at Clubhotel Riu Funana in the Santa Maria resort, Sal, Cape Verde. A bathing injury has occurred at the beach adjacent to the Clubhotel Riu Funana, and this report seeks to estimate the wave and beach morphology conditions at the time of the bathing incident, as well as to identify typical bathing conditions that occur throughout the year at the beach.

Through a process of expert judgement using a combination of wave analysis, and assessment of in-situ and satellite imagery, the beach at Riu Funana beach is expected to sit within the ‘reflective’ or ‘low tide terrace’ end of the beach morphology spectrum. The likely beach profile gradient in the area of wave breaking is expected to be 0.1 (slope of 1-in-10), which represents a steep beach profile.

Steep beaches exposed to small wave heights with long wavelengths experience plunging or collapsing/surging wave breakers. Such waves break intensely across a narrow region of beach, with collapsing/surging waves breaking right at the shoreline. Given the expected beach morphology and wave breaker types, shore-break impact injuries are expected to be the primary beach hazard type at Riu Funana beach.

From processed wave model data, maximum breaking wave heights (defined here as the largest individual wave occurring in a given period of time) at the site are predicted to vary between 0.5 and 7.0 m, but only exceed 2.3 m 10% of the time. Wave breaking is predicted to be predominantly within the ‘plunging’ regime, but periods characterised by ‘collapsing’ and ‘surging’ breakers are also evident. These represent the most powerful of the wave breaker types.

In-situ photographs of waves breaking at Clubhotel Riu Funana confirm that waves typically break very close to the beach, and even the larger waves (breaking wave height, $H_b > 1$ m) break as plunging breakers with considerable breaking intensity and power at the shoreline.

On the day of the bathing incident on the 31st March 2018, wave heights are predicted to have been similar to the annual-average significant breaking wave height but lower than the seasonal-average breaking wave height for the season in which the incident occurred (winter). Accounting for uncertainties in the wave conditions and beach slope, there is 95% confidence that the breaker type was plunging, collapsing, or surging around the time of the incident, with the largest individual wave around the time of the incident (estimated to be approximately 1.3 m in height) predicted to have been either plunging or collapsing as it broke. The combination of wave height and period at the time of the

bathing incident sits within a transitional range representing the overlap between wave conditions typically associated with yellow flags and those associated with red flags flown at the beach during March and April of 2018.

Contents

1. Introduction.....	1
2. Site Morphology and physical hazards	4
3. Site Wave Climate	9
4. Conditions on the day of the bathing incident	18
5. Analysis of wave conditions and lifeguard flags	21
6. Conclusions.....	25
References.....	27
Appendix A. Expertise of the CMAR team.....	28
Appendix B. Processing of wave model data.....	31
Appendix C. Breaker type distributions.....	33

Table of Figures

Figure 1-1. Clubhotel Riu Funana, Santa Maria resort, Sal Island, Cape Verde	1
Figure 1-2. Location maps showing Cape Verde off the west African coast (upper left), Sal island to the North East of Cape Verde (upper centre), the Santa Maria area at the southern tip of the island (upper right), and the Clubhotel Riu Funana - Santa Maria resort beach, west of Santa Maria city, Sal island (lower).	2
Figure 1-3. Chart of bathymetric depth in the Cape Verde island chain, from the General Bathymetric Chart of the Oceans (GEBCO) database (https://www.gebco.net/). Santa Maria on the island of Sal is demarked with a red star. Note that the coastal shelf visible around Sal Island is less than 100 m depth.....	3
Figure 2-1. Beach morphology types for microtidal beaches, identified by Wright and Short (1984). The red box indicates the most likely beach morphology types to occur at Riu Funana beach, Santa Maria, Sal, Cape Verde.....	6
Figure 2-2. Sentinel-2 satellite imagery of Clubhotel Riu Funana, Santa Maria, Sal, Cape Verde showing (from top to bottom) low to high energy wave conditions, respectively, and the full range of surf-zone width (visible as a band of white-water) from the 326 images between September 2015 and June 2021. Panel A shows typical surf-zone width, while panels D and E show the widest surf-zone..	7
Figure 2-3. Aerial imagery of Riu Funana beach showing beach cusp formations at the shoreline.....	8
Figure 2-4. Photograph of beach sediment at Riu Funana beach, extracted from a tourist photograph posted on Google Maps.	8
Figure 3-1. Wave model output location at 16.6° latitude, -23° longitude, approximately 7.5 km directly offshore of Riu Funana beach, in deep water (>1000 m depth).....	11
Figure 3-2. Wave roses showing proportion of significant wave heights (left) and wave periods (right) from different directional sectors at the wave model output location.....	12
Figure 3-3. Cross-sectional representation of the three main types of breaking waves: spilling, plunging, and surging. At the interface between plunging and surging conditions, ‘collapsing’ wave breaking occurs, involving intense wave breaking occurring at the shore.....	12
Figure 3-4. Wave hindcast time series from the WAVERYS global wave model, output in deep water approximately 7.5 km offshore of Riu Funana beach. Vertical dashed lines show the date on which the beach incident occurred. The horizontal dashed lines in the lower panel show the thresholds that differentiate between spilling, plunging, and surging breakers. Black lines in each panel show a monthly moving average for each plotted parameter. MWD is the mean wave direction from shore normal.	13

Figure 3-5 Examples of wave breaking at Praia de Lacacao under ‘low wave energy’ conditions (estimated as $0 < H_b < 0.5$ m). 15

Figure 3-6. Examples of wave breaking at Riu Funana beach under ‘medium wave energy’ conditions (estimated as $0.5 < H_b < 1$ m)..... 16

Figure 3-7. Examples of wave breaking at Riu Funana beach under ‘upper wave energy’ conditions (estimated as $H_b > 1$ m)..... 17

Figure 4-1. Wave hindcast time series from the WAVERYS global wave model, output in deep water approximately 7.5 km offshore of Riu Funana beach, for the 7-day period centred on the day of the incident. Vertical dashed lines show the likely period within which the incident took place on the 31st of March 2018 (6 am – 10 pm). The horizontal dashed lines in the lower panel show the thresholds that differentiate between spilling, plunging, and surging/collapsing breakers. 20

1. Introduction

Coastal Marine Applied Research (CMAR) have been commissioned by Adam Wooler to assess physical bathing hazards at Clubhotel Riu Funana in the Santa Maria resort, Sal, Cape Verde (Figure 1-1). A bathing injury (herein also referred to as ‘the bathing incident’) occurred at the beach adjacent to the Clubhotel Riu Funana (herein also referred to as ‘the hotel’), and this report seeks to estimate the wave and beach morphology conditions at the time of the bathing incident, as well as to identify typical bathing conditions that occur throughout the year at the beach. Riu Funana beach is situated on the western side of the Santa Maria resort which is on the south of Sal, one of the Cape Verde islands, off the western coast of Africa in the Atlantic Ocean. The hotel is situated at a latitude of approximately 16.6 °N and longitude of 22.9°W. The beach is at the location of the Clubhotel Riu Funana and faces an orientation of 275° from North (Figure 1-2).

The beach has a small ‘microtidal’ tide range of 0.8 m during an average spring tide (From Admiralty Total Tide data at the secondary harmonic tidal port of Ilha Do Sal Bahia De Palmeira). There is a relatively shallow coastal shelf (< 100 m depth) surrounding the island of Sal (Figure 1-3).



Figure 1-1. Clubhotel Riu Funana, Santa Maria resort, Sal Island, Cape Verde



Figure 1-2. Location maps showing Cape Verde off the west African coast (upper left), Sal island to the North East of Cape Verde (upper centre), the Santa Maria area at the southern tip of the island (upper right), and the Clubhotel Riu Funana - Santa Maria resort beach, west of Santa Maria city, Sal island (lower).



Figure 1-3. Chart of bathymetric depth in the Cape Verde island chain, from the General Bathymetric Chart of the Oceans (GEBCO) database (<https://www.gebco.net/>). Santa Maria on the island of Sal is demarked with a red star. Note that the coastal shelf visible around Sal Island is less than 100 m depth.

2. Site Morphology and physical hazards

Beach morphology is a key driver of physical beach hazards, and the planform and profile shape of a beach determines to a large degree which physical hazards are likely to be encountered. The two primary causes of surf zone injuries and drownings worldwide are rip currents and shore-break waves (Castelle *et al.*, 2019). Rip currents are dangerous flows that can take bathers from the shallows out to sea and cause hundreds of drownings and tens of thousands of beach rescues (~70%) globally each year (Castelle *et al.*, 2016). Shore-break waves feature concentrated and intense breaking of waves at the shoreline and tend to cause impact injuries such as bone fractures and spinal injuries, but make up a smaller proportion of surf-zone injuries globally (Castelle *et al.*, 2019). While rip currents are found predominantly on beaches in the ‘intermediate’ beach morphology range (Figure 2-1) and are typically driven by bathymetric channels in the beach face, shore-break waves typically occur on steep beach profiles, and are therefore more commonly associated with ‘reflective’ beach types (Figure 2-1) or with the steep upper (high-tide) part of the profile of intermediate beach types.

Beach topographic/bathymetric survey data (for example measured profiles) were not available for this analysis, so it is impossible to be certain about the beach profile and gradient at the beach, especially at the time of the bathing incident. Instead, the beach morphology at Riu Funana beach was assessed through a process of expert judgement using a combination of wave analysis (Section 3), and assessment of in-situ imagery (from Google Maps photographs) and satellite imagery (Sentinel-2 images covering September 2015 – June 2021). From this analysis, it was concluded that **the Riu Funana beach sits consistently within the ‘reflective’ or ‘low tide terrace’ morphology types** (see Figure 2-1 for beach morphology types). This was determined from the following evidence:

- The satellite imagery shows a consistently narrow surf-zone (Figure 2-2), void of visible rip currents or channels. The surf-zone is 0 – 20 m wide for more than 90% of the 326 available Sentinel-2 images, and only exceeded 50 m width twice during extreme wave conditions. This is a clear indication of a steep reflective beach type, as shallow beach profiles consistently exhibit wide surf-zones, > 50 m wide, even during modest wave conditions.
- Active beach cusps are visible in 7 out of 10 available Google Earth aerial images between October 2003 and September 2019 (Figure 2-3), and are features that are typically found on steep beaches in the upper intermediate to reflective morphology range (i.e. panels e-f, Figure 2-1).
- The dimensionless fall velocity, Ω , is a parameter often used to estimate beach morphological state (Wright and Short, 1984; Masselink and Short, 1993). This can be computed from the

average significant breaking wave height ($H_b = 0.9$ m, from Table 3-2, Section 3), the average wave period ($T = 10.2$ s, from Table 3-2, Section 3), and using an estimated sediment fall velocity (ω_s), as $\Omega = H_b / \omega_s T$. From expert assessment of tourist photographs of the beach (for example, Figure 2-4), the sediment is likely to consist of ‘medium sand’ with a grain size on the order of 0.25 – 0.5 mm diameter, which, following Van Rijn (1993), indicates ω_s is likely to sit within the range of 0.03 – 0.065 m/s. This yields average values for Ω of 1.4 – 2.9, which is within the ‘reflective’ and ‘low tide terrace’ beach state range (Wright and Short, 1984; Wright *et al.*, 1985; Masselink and Short, 1993).

The beach profile gradient is an important consideration in this report, as this parameter strongly influences the intensity of wave breaking at the shore and is used to assess the variability in breaker types in Section 3 and Section 4 of the report. Tourist photographs of the beach indicate the sediment is likely to consist of ‘medium sand’ (for example, Figure 2 4) with a grain size on the order of 0.25 – 0.5 mm diameter. From data presented by Bujan *et al.* (2019), such grain sizes are typically found on beaches with slopes of 0.05 (1-in-20) to 0.1 (1-in-10). Furthermore, reflective and low tide terrace morphology types typically have steep gradients, on the order of 0.05 – 0.2 at the shoreline (Wright and Short, 1984; Masselink and Short, 1993), and typically around 0.1 (1-in-10) where wave breaking occurs. Therefore, we consider **the likely beach profile gradient in the area of wave breaking at Riu Funana beach to be approximately 0.1 (slope of 1-in-10)**, although acknowledge that there will be a degree of temporal and spatial variability in the slope and uncertainty in its estimation (accounted for in Section 4).

Such beach gradient values have previously been associated with shore-break waves and impact injuries in the scientific literature (Castelle *et al.*, 2019). **Given the steep beach gradient, inferred from the likely sediment and morphology of the beach, shore-break impact injuries are expected to be the primary beach hazard type at Riu Funana beach.** Rip currents are not likely to be a common beach hazard at Riu Funana beach, as reflective beaches lack subtidal bathymetric channels that are the most common cause of rip currents (Castelle *et al.*, 2019). however, spatially variable backwash from beach cusps can result in small offshore pulses of water exiting the surf-zone known as ‘swash-rips’ (Castelle *et al.*, 2016) and these may occur at Riu Funana beach during energetic wave conditions (i.e., $H_b > 1$ m), but are considered by Castelle *et al.* (2016) to pose only a limited bathing hazard due to their small scale.

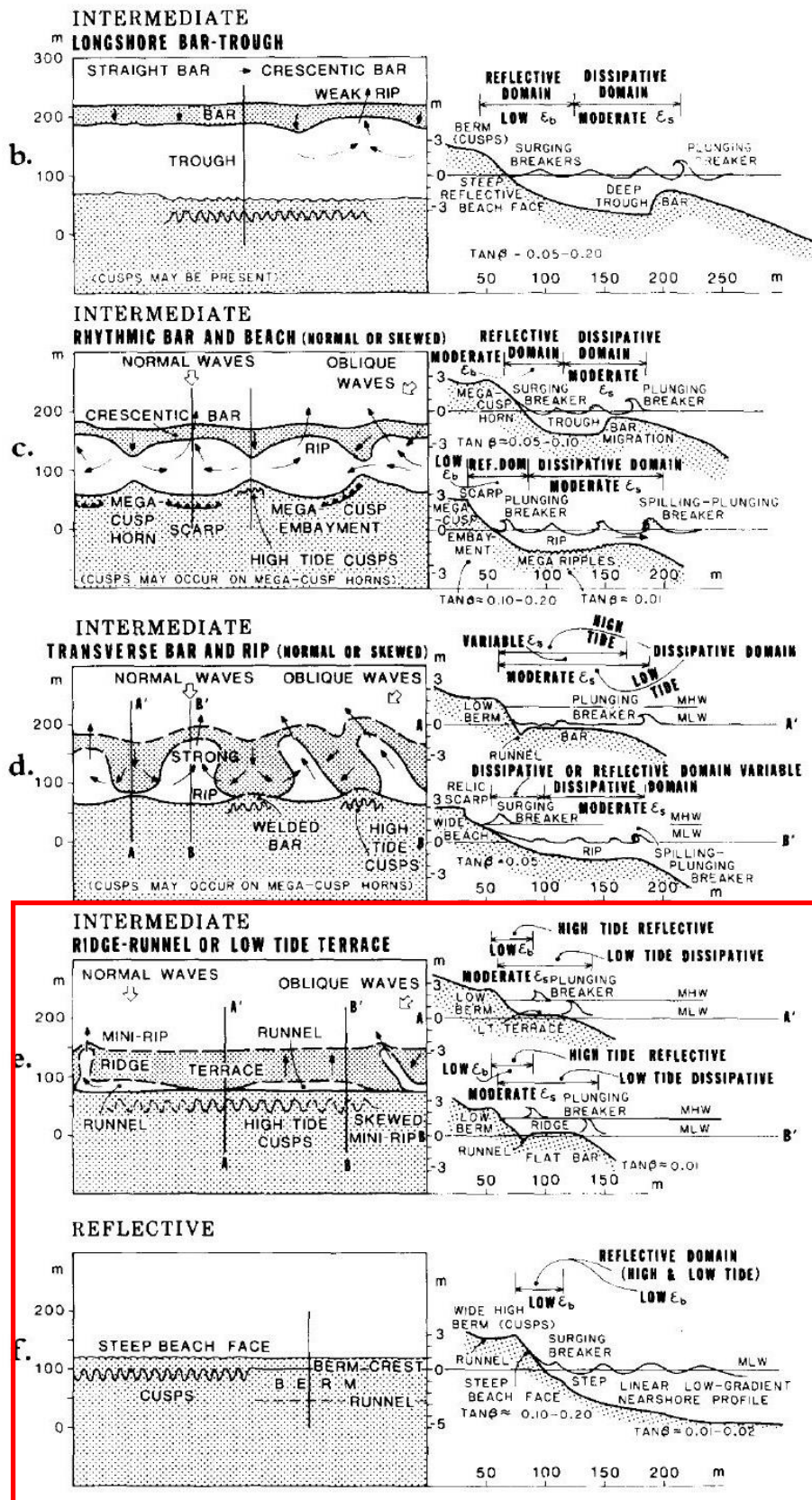


Figure 2-1. Beach morphology types for microtidal beaches, identified by Wright and Short (1984). The red box indicates the most likely beach morphology types to occur at Riu Funana beach, Santa Maria, Sal, Cape Verde.

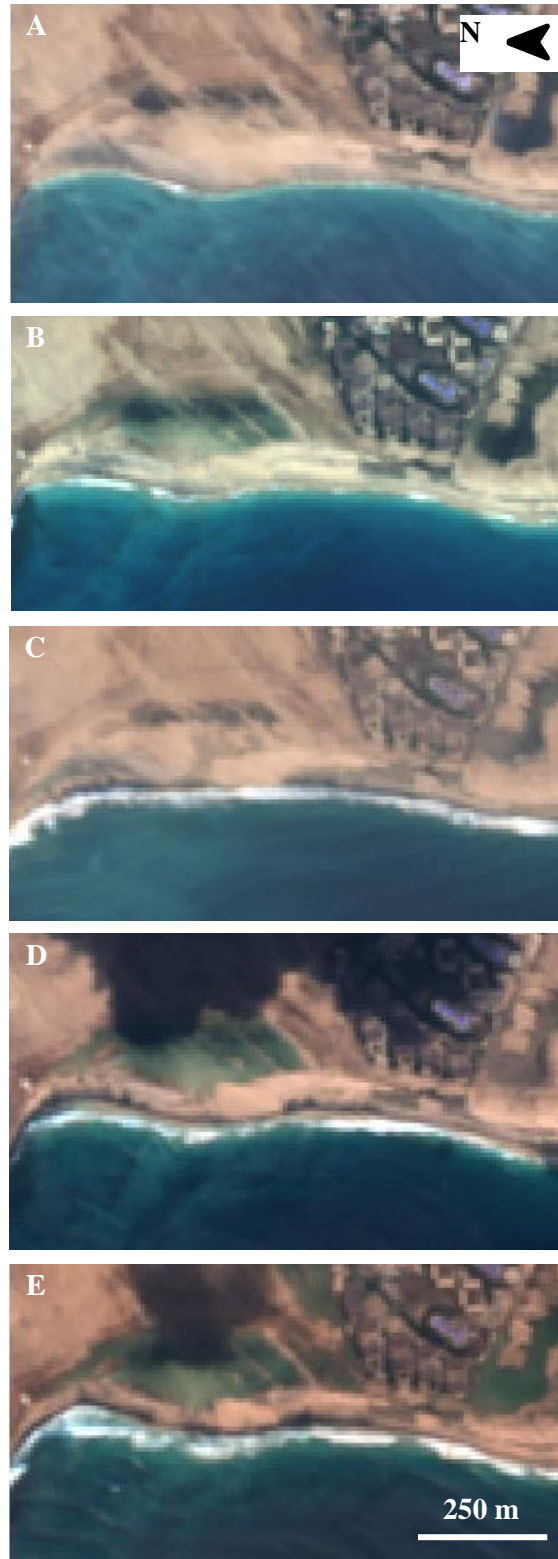


Figure 2-2. Sentinel-2 satellite imagery of Clubhotel Riu Funana, Santa Maria, Sal, Cape Verde showing (from top to bottom) low to high energy wave conditions, respectively, and the full range of surf-zone width (visible as a band of white-water) from the 326 images between September 2015 and June 2021. Panel A shows typical surf-zone width, while panels D and E show the widest surf-zone.



Figure 2-3. Aerial imagery of Riu Funana beach showing beach cusp formations at the shoreline.



Figure 2-4. Photograph of beach sediment at Riu Funana beach, extracted from a tourist photograph posted on Google Maps.

3. Site Wave Climate

The most common directions from which waves arrive offshore of the Riu Funana beach is from the north and north-east, driven by the north-east trade winds at this latitude; however waves also arrive less frequently from the north-north-west (Figure 3-2). Waves arriving from the north-east will largely be blocked by the presence of Sal Island itself; however, the relatively shallow coastal shelf surrounding Sal (< 100 m depth; Figure 1-3) is expected to induce wave refraction, allowing some wave energy from the north to propagate into Riu Funana beach. Wave data for Cape Verde are extremely limited, with no historical wave buoy measurements available within or close to the island chain. Therefore, wave model data were used for the present analysis.

Wave model hindcast data were extracted from the global ocean reanalysis wave system of Météo-France (WAVERYS) with a spatial resolution of $1/5^\circ$ degree (approximately 20 km), which provides global wave model data for ocean sea surface waves covering the period 15th Jan 1993 – 25th Dec 2018. These data are provided freely through the Copernicus Marine Environment Monitoring Service (CMEMS, <https://marine.copernicus.eu/>). Model data were extracted at a location of 16.6° latitude, -23° longitude (Figure 3-1), which is approximately 7.5 km directly offshore of Riu Funana beach, in deep water (~1000 m depth). The wave model data for the entire hindcast period were processed and used to estimate breaking wave conditions at the beach, using the methods described in Appendix B.

At a given time and location, a multitude of waves of differing heights and frequencies occur in the ocean. Significant wave heights and maximum wave heights are presented in this analysis. The significant wave height is the average height of the highest one-third of waves in a given sea state, while the maximum wave height represents the largest individual wave in the sea state and can be approximately double the significant wave height (see Appendix B for more details). Despite being infrequent, it is important to consider the maximum wave height when determining beach hazards, as an injury could occur due to the single largest wave during a given period of time. While significant wave height is provided by the wave model, the maximum wave height is not a parameter provided explicitly by the wave model and has been derived for this report from the significant wave height using an established statistical relationship (method detailed in Appendix B).

Breaking waves can vary in shape and intensity between gentle ‘spilling’ breakers that dissipate their wave energy gradually over the beach profile, to ‘plunging’ breakers that break intensely over a short part of the beach profile, and finally to ‘surging’ waves that break or reflect their energy entirely at the shoreline. At the interface between plunging and surging conditions, ‘collapsing’ wave breaking occurs, involving intense wave breaking occurring at the shore. To estimate the type of wave breaking

occurring at a given time (Figure 3-3), the Iribarren Number, ξ , was calculated (Appendix B), which is a well-established parameter used to predict the occurrence of either spilling, plunging, or collapsing/surging breakers, given information on beach slope and wave steepness (Iribarren and Nogales, 1949; Battjes, 1974). The thresholds of the Iribarren Number that differentiate different wave breaker types are shown in Table 3-1. Small values for ξ (i.e. $\xi < 0.4$) are attained when the beach has a gentle gradient and the incident wave field is characterized by a large wave height and a short wave length (or short wave period - the interval between each wave crest arriving at the beach). Such conditions promote the formation of gently spilling breakers. Large values of ξ (i.e. $\xi > 2$) are found when the beach is steep and the incident wave field is characterized by a small wave height and a long wave length (or long wave period). Such conditions favour the formation of surging breakers. Plunging breakers prevail when $\xi = 0.4 - 2$. At the interface between plunging and surging conditions ($\xi \approx 2$), collapsing breakers occur, involving intense wave breaking occurring at the shore.

The Iribarren Number was calculated for the entire wave hindcast period using the modelled significant breaking wave height, peak wave period, and the estimated representative beach gradient determined in Section 2 ($\tan \beta = 0.1$).

The entire time-series of wave conditions at Riu Funana beach from the WAVERYS wave model are presented in Figure 3-4, and are presented again in Figure 4-1 for a 7 day period centred on the day the bathing incident in question occurred. Summary wave statistics are presented in Table 3-2 and Table 3-3. From the processed wave data, significant breaking wave heights at the site are expected to vary from 0.3 – 4.4 m (Figure 3-4), but do not often exceed 1.4 m, with only 10% of the wave data exceeding this value (Table 3-3). Maximum breaking wave heights at the site are expected to vary from 0.5 – 7.0 m (Figure 3-4), but do not often exceed 2.3 m, with only 10% of the wave data exceeding this value (Table 3-3).

Wave conditions do vary throughout the year, with mean summer and winter significant breaking wave heights varying from 0.7 – 1.1 m, with peak wave periods of 8.8 – 11.5 s (Table 3-2). Breaker type is predicted to be ‘plunging’ on average ($\xi = 0.4 - 2$; Table 3-2); however, periods characterised by ‘collapsing’ ($\xi \approx 2$) and ‘surging’ ($\xi > 2$) breakers are evident in the timeseries in Figure 3-4. However, over any period of time a range of wave breaker types occur, due to variations in wave height and period occurring in any given sea state.



Figure 3-1. Wave model output location at 16.6° latitude, -23° longitude, approximately 7.5 km directly offshore of Riu Funana beach, in deep water (>1000 m depth).

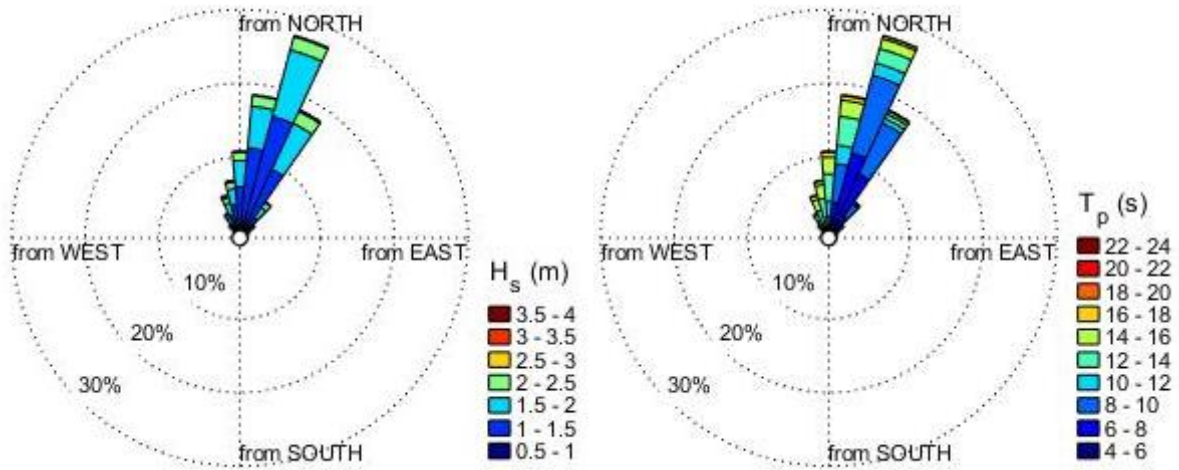


Figure 3-2. Wave roses showing proportion of significant wave heights (left) and wave periods (right) from different directional sectors at the wave model output location.

Table 3-1. Thresholds of Iribarren Number, ξ , used to differentiate between spilling, plunging, and collapsing/surging breakers. At the interface between plunging and surging conditions, ‘collapsing’ wave breaking occurs, involving intense wave breaking occurring at the shore.

Breaker type	ξ range
Spilling	$\xi < 0.4$
Plunging	$0.4 \leq \xi \leq 2$
Surging	$\xi > 2$

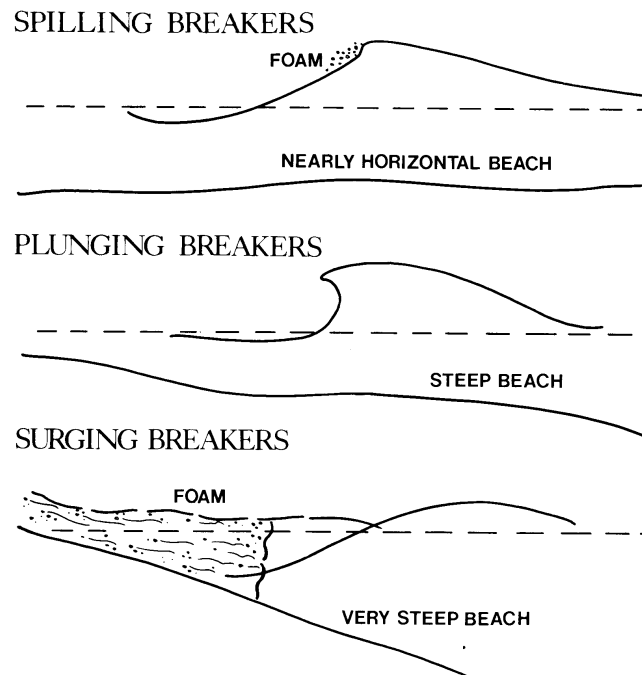


Figure 3-3. Cross-sectional representation of the three main types of breaking waves: spilling, plunging, and surging. At the interface between plunging and surging conditions, ‘collapsing’ wave breaking occurs, involving intense wave breaking occurring at the shore.

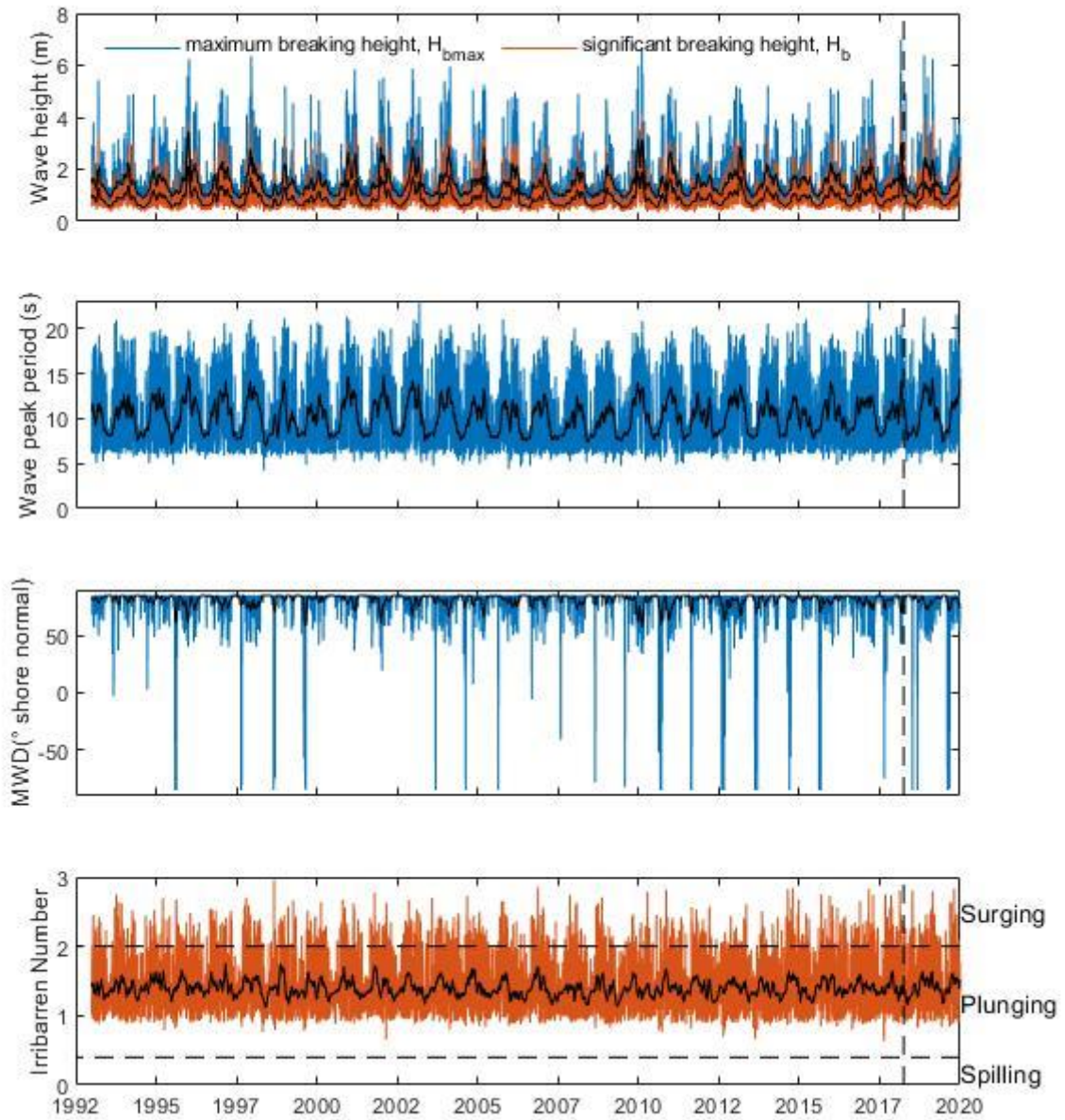


Figure 3-4. Wave hindcast time series from the WAVERYS global wave model, output in deep water approximately 7.5 km offshore of Riu Funana beach and shoaled to breaker height using linear wave theory and refraction. Vertical dashed lines show the date on which the beach incident occurred. The horizontal dashed lines in the lower panel show the thresholds that differentiate between spilling, plunging, and surging breakers. Black lines in each panel show a monthly moving average for each plotted parameter. MWD is the mean wave direction from shore normal.

Table 3-2. Average (mean) wave conditions at Riu Funana beach, Sal, Cape Verde, determined from the processed WAVERYS wave model data. The summer averaging period was April – September, inclusive, and winter averaging period was October – March, inclusive.

Averaging period	Maximum breaking wave height (m)	Significant breaking wave height (m)	Wave peak period (s)	Iribarren Number ($\tan \beta = 0.1$), breaker type	Dim. Fall velocity ($\omega_s = 0.03 - 0.065$ m/s)
All	1.5	0.9	10.2	1.1, plunging	1.4 – 2.9
Summer	1.2	0.7	8.8	1.0, plunging	1.2 – 2.7
Winter	1.7	1.0	11.5	1.1, plunging	1.5 – 3.2

Table 3-3. 10% and 90% percentile wave conditions at Riu Funana beach, Sal, Cape Verde, determined from the processed WAVERYS wave model data.

Percentile	Maximum breaking wave height (m)	Significant breaking wave height (m)	Peak wave period (s)	Iribarren Number ($\tan \beta = 0.1$), breaker type	Dim. Fall velocity ($\omega_s = 0.03 - 0.065$ m/s)
10%	0.9	0.5	6.7	1.05, plunging	1.2 – 2.6
90%	2.3	1.4	14.7	1.84, plunging	1.5 – 3.2



Figure 3-5 Examples of wave breaking at Praia de Lacacao under ‘low wave energy’ conditions (estimated as $0 < H_b < 0.5$ m).



Figure 3-6. Examples of wave breaking at Riu Funana beach under 'medium wave energy' conditions (estimated as $0.5 < H_b < 1$ m).

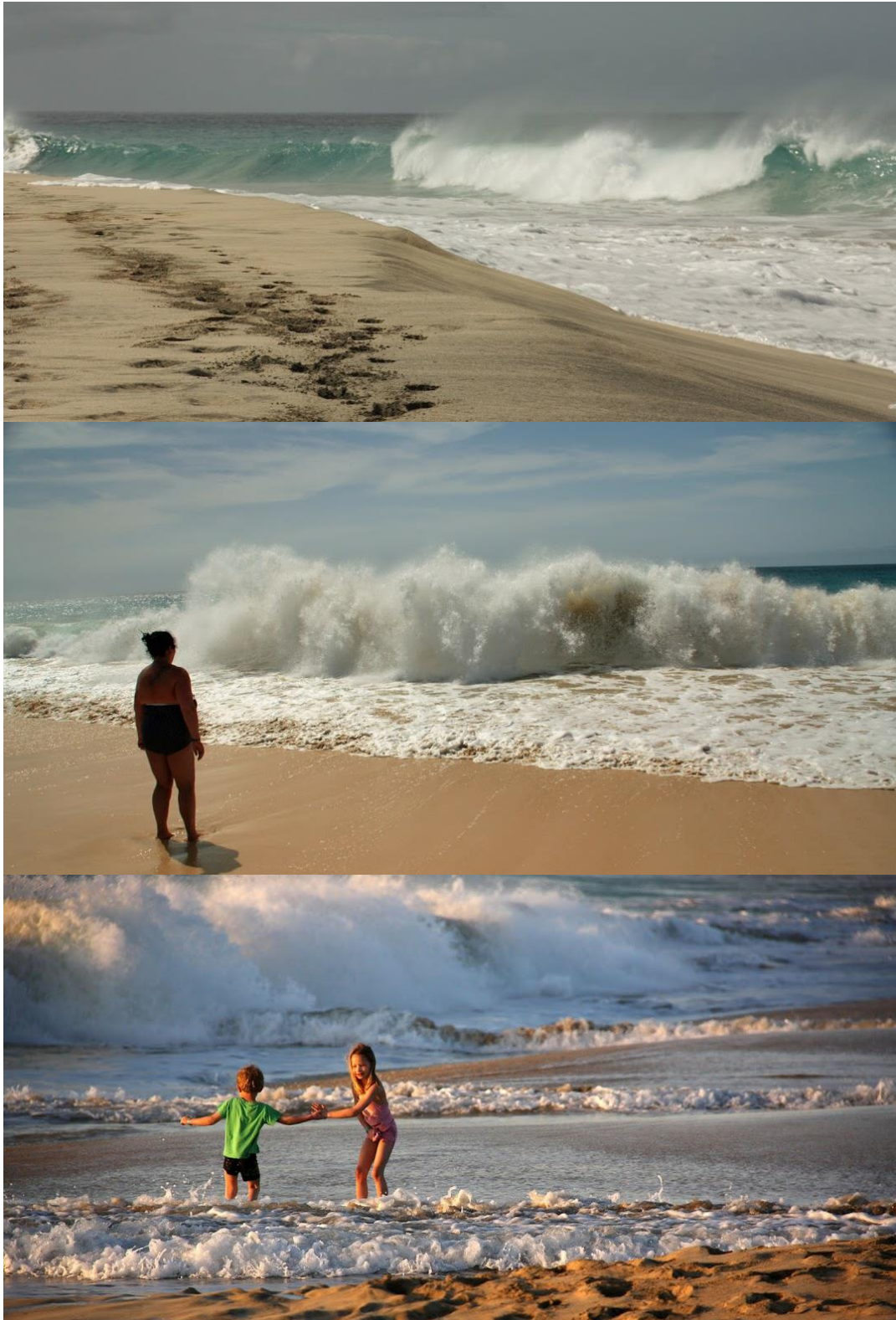


Figure 3-7. Examples of wave breaking at Riu Funana beach under 'upper wave energy' conditions (estimated as $H_b > 1$ m).

4. Conditions on the day of the bathing incident

From the processed wave model data, the likely wave conditions on the day of the bathing incident in question can be extracted (31st March 2018). The wave conditions near the time of the bathing incident is summarised in Table 4-1, and a time-series plot of wave conditions over the 7-day period centred on the time of the incident are presented in Figure 4-1. The wave model data has a three-hourly temporal resolution, and the time of the incident is at 11:30am. The wave conditions presented in Table 4-1 are at the closest model time to the incident (12:00pm). The conditions are shown to be relatively similar throughout the day of the incident (Figure 4-1).

During the incident, wave conditions (Table 4-1) are predicted to have been at the level similar to the annual average significant breaking height, and lower than the winter average significant breaking wave height (Table 3-2), which is the season in which the incident occurred, with $H_b = 0.8 \text{ m}$ and $H_{bmax} = 1.3 \text{ m}$. The type of wave breaking occurring on the day of the incident is a key factor, as this dictates the likelihood of shore-break impact injuries. However, to be confident about the type of wave breaking occurring at the beach, various uncertainties must be accounted for, including:

- uncertainty in the prediction of wave height
- uncertainty in the prediction of wave period
- uncertainty in the beach slope at the exact time and location of the incident

Therefore, for this analysis we calculate a range of possible values for ξ in order to explore the likely range of breaking that was occurring on the day of the incident. To do this, the predicted wave height and period on the day of the incident (Table 4-1), and estimated beach slope ($\tan \beta = 0.1$), are each assumed to be accurate to within +/- 50% of the actual values occurring on the day (a highly conservative range). To generate confidence bounds based on these values, a simple triangular probability distribution function (PDF), centred around the estimated values for wave height, period, and beach slope, was used to describe the likelihood of values being up to 50% higher or lower than the estimated values, and then a monte-carlo approach was used to randomly sample 10,000 values from within the PDFs of each variable. Using these randomly sampled values, the distribution of likely ξ values was determined (Appendix C), allowing confidence bounds for ξ , and therefore breaker type, to be determined.

As the type of wave breaking occurring on the day of the incident depends strongly on which wave heights within the sea state are considered, this analysis was repeated using root-mean-square average (H_{rms}), significant (H_s), and maximum (H_{max}) breaker heights predicted for the day of the incident.

From this analysis, the median breaker type on the day of the incident is predicted to be within the plunging regime regardless of whether the average, significant, or maximum wave height is considered. Using the upper and lower confidence bounds, it can also be stated that **there is 95% confidence that the breaker type was plunging, collapsing, or surging, with the largest individual wave on the day either plunging or collapsing as it broke.**

Table 4-1 Predicted wave conditions at Riu Funana beach, Sal, Cape Verde near the time (12:00) of the bathing incident, determined from the processed WAVERYS wave model data.

Incident Date	Maximum Breaking wave height, H_{max} (m),	Significant Breaking wave height, H_s (m),	Average breaking wave height, H_{rms} (m),	Wave direction from (degrees from north)	Wave direction from (degrees from shore normal)	Breaking wave direction from (degrees from shore normal)	Peak wave period (s)
31 st March 2018, time unconfirmed	1.3	0.8	0.6	4	85	11	10

Table 4-2 Predicted wave breaker types at Riu Funana beach, Sal, Cape Verde on the day of the bathing incident, determined from the processed WAVERYS wave model data. Breaker types are shown for different wave heights likely to have been present on the day (Table 4-1). The breaker type range was determined from the 95% confidence interval of the Iribarren value.

	Largest individual wave (H_{max})	Average of largest 1/3 rd of waves (H_s)	Average wave (H_{rms})
Median Iribarren, ξ , (95% confidence range)	1.2 (0.5 – 2.3)	1.5 (0.7 – 2.9)	1.8 (0.8 – 3.4)
Breaker type range	plunging, collapsing, surging	Plunging, collapsing, surging	Plunging, collapsing, surging

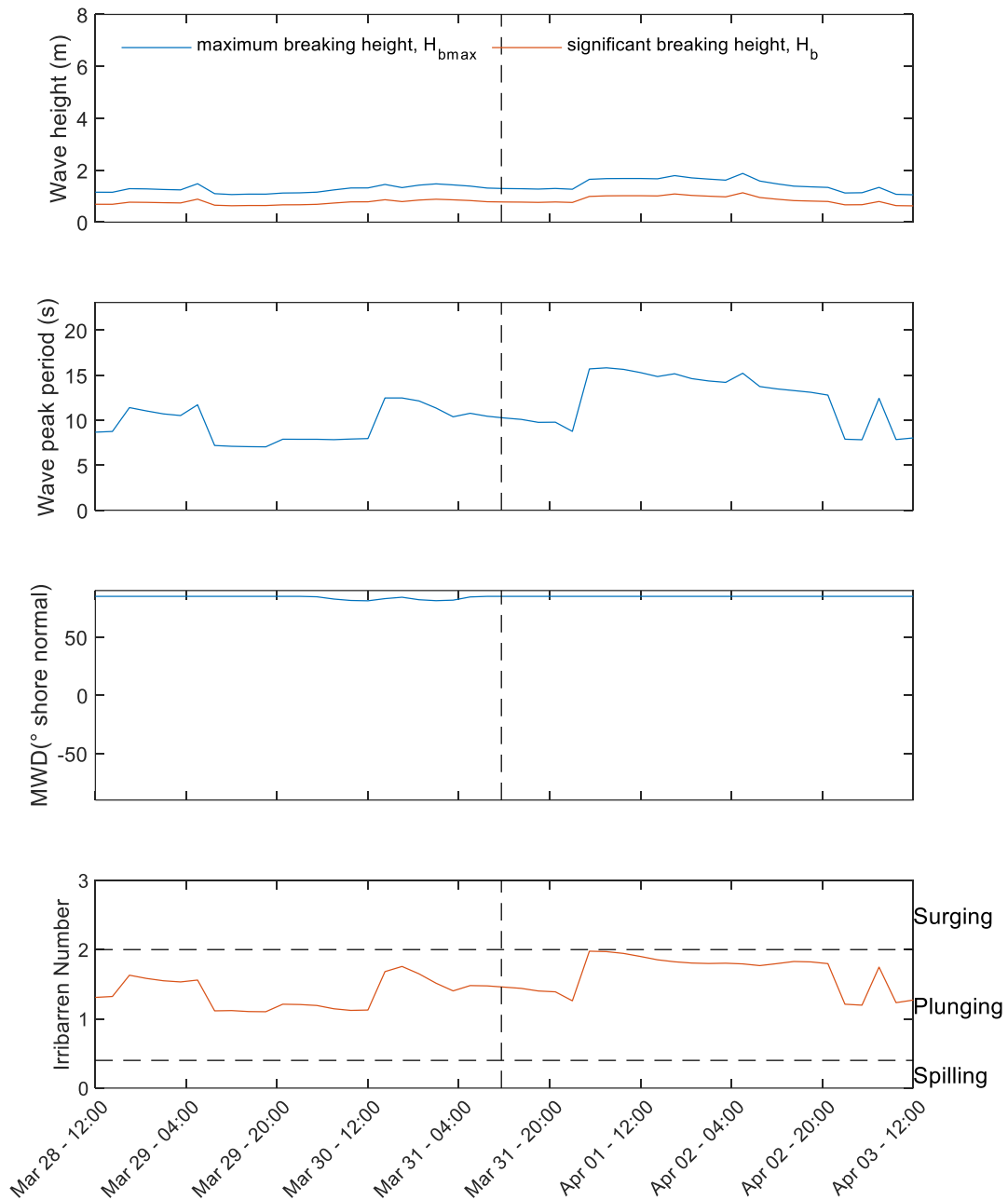


Figure 4-1. Wave hindcast time series from the WAVERYS global wave model, output in deep water approximately 7.5 km offshore of Riu Funana beach and shoaled to breaker height using linear wave theory and refraction, for the 7-day period centred on the day of the incident. Vertical dashed lines show the time the incident took place on the 31st of March 2018. The horizontal dashed lines in the lower panel show the thresholds that differentiate between spilling, plunging, and surging/collapsing breakers.

5. Analysis of wave conditions and lifeguard flags

Using the lifeguard hazard flag log from Riu Funana beach over March and April 2018, wave conditions associated with the yellow and red flags issued by the lifeguards during the morning and afternoon periods of each day can be assessed. As the exact timing of the lifeguard morning and afternoon periods are not explicit in the lifeguard logs, it was assumed that the lifeguard service was split into a four-hour morning period from 9am to 1pm and a four-hour afternoon period from 1pm to 5pm. For each morning or afternoon period in the log, a flag colour is recorded, indicating the colour of the lifeguard flag(s) displayed on Riu Funana beach during that period of time. There is a relatively even divide between the number of yellow flags and red flags that were issued during the 122 recorded half-day periods in March and April 2018, with slightly more yellow flags issued (69 of the 122 half-day periods, or 57%) than red flags (53 of the 122 half-day periods, or 43%).

The wave conditions that occurred during each of the recorded flags can be extracted from the previously described wave model dataset, and are shown in Figure 5-1. Using the previously described four-hour morning and afternoon periods on each day, the average (median) wave condition during each flag period was extracted from the data, representing a best-estimate of the wave conditions that informed the choice of flag flown during each period. Histograms showing the distribution of wave conditions associated with each of the flags flown are shown in Figure 5-2. The average (median) wave condition associated with each flag flown during March and April of 2018 is presented in Table 5-1, alongside the estimated conditions at the time of the bathing incident on 31st March 2018.

During March and April of 2018, red flags tended to be flown during larger waves (significant breaking wave heights on average 1.36 m and maximum individual breaker heights of 1.3-6.3 m), with longer wave periods (on average 14 s, ranging between 7.5-19 s). All of the wave conditions that had periods above 10 s and significant wave heights above 1.5 m (representing a high level of wave power) are associated with a red flag. Yellow flags tended to be flown during smaller waves (significant breaking wave heights on average 0.8 m and maximum individual breakers of 1.1-2.1 m) with shorter periods (<10 s), representing lower wave power conditions than those during red flags, albeit with some potentially large individual breakers occurring. It is estimated that the breaker type was entirely in the plunging or surging/collapsing regimes during March and April of 2018; however, given the range of probable beach slopes at different stages of tide (Figure 2-1), it is possible that some large and short period breakers may have occasionally been gently spilling at some stages of the tide. 15 of the 122 recorded flags were yellow flags flown when wave period was greater than 10 s and significant breaker heights were between 0.8-1.3 m, representing quite powerful breaking waves. Furthermore, 19 of the 122 recorded flags were red flags flown under the exact same range of wave

conditions. This range of conditions is a transitional range representing the overlap between wave conditions typically associated with red and yellow flags in March and April of 2018. The overlap consists of 34 flag periods of the 122 in the log (28%).

While the bathing incident on the 31st of March 2018 occurred during relatively modestly sized breakers (0.8 m significant height, largest individual breaker approximately 1.3 m) typical of the other yellow flag conditions during March and April 2018, the combination of wave height and period (that contribute to the overall power of the waves) sits within the transitional range representing the overlap between wave conditions typically associated with red and yellow flags. The breaker type is also estimated with 95% confidence to have been plunging, collapsing, or surging at the time of the incident (Section 4), representing forms of wave breaking that have previously been associated with surfzone impact injuries (Castelle *et al.*, 2019).

Table 5-1. Average (median) wave conditions associated with each lifeguard flag flown during March and April of 2018, compared to wave conditions at the time of the bathing incident on 31st March 2018. Values shown to 2 significant figures.

	Average yellow flag (range for March and April 2018)	Average red flag, (range for March and April 2018)	Incident conditions, 31 st March 2018
Significant breaking height, H_s (m)	0.8 (0.6 – 1.3)	1.4 (0.8 – 3.9)	0.8
Maximum breaking height, H_{max} (m)	1.4 (1.1 – 2.1)	2.2 (1.3 – 6.3)	1.3
Wave peak period (s)	8.4 (6.1 – 18)	14 (7.5 – 19)	10
Breaking wave direction from (degrees from shore normal)	14 (7.4 – 17)	11 (7.4 – 18)	11
Iribarren Number computed from H_s	1.2 (1 – 2.2)	1.3 (0.9 – 2.1)	1.5

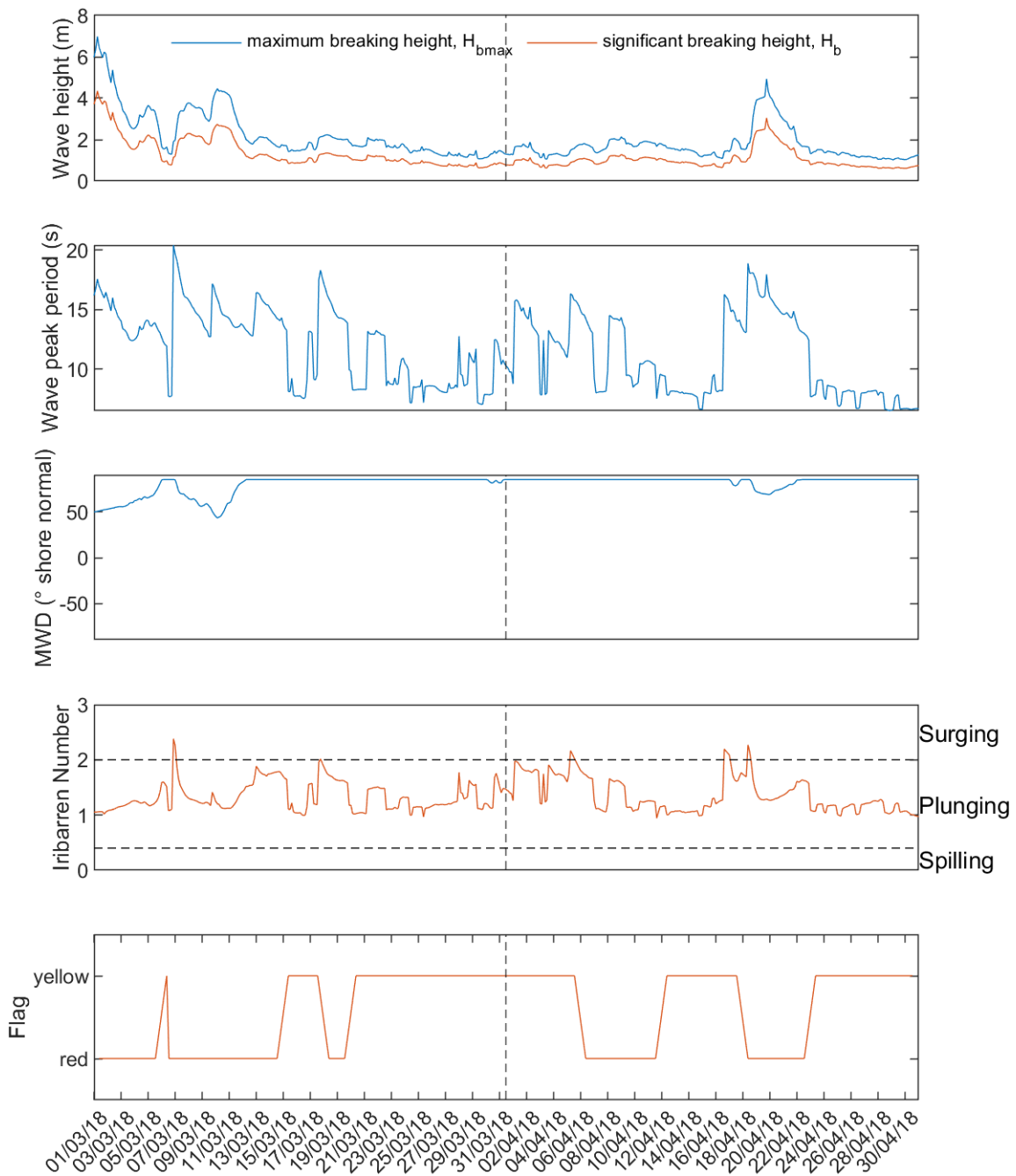


Figure 5-1. Time series of lifeguard flags (lower panel) and associated wave hindcast time series from the WAVERYS global wave model, output in deep water approximately 7.5 km offshore of Riu Funana beach and shoaled to breaker height using linear wave theory and refraction (upper panels), for the 2-month period centred on the day of the incident (31st of March 2018; vertical dashed line). The horizontal dashed lines in the fourth panel show the thresholds that differentiate between spilling, plunging, and surging/collapsing breakers.

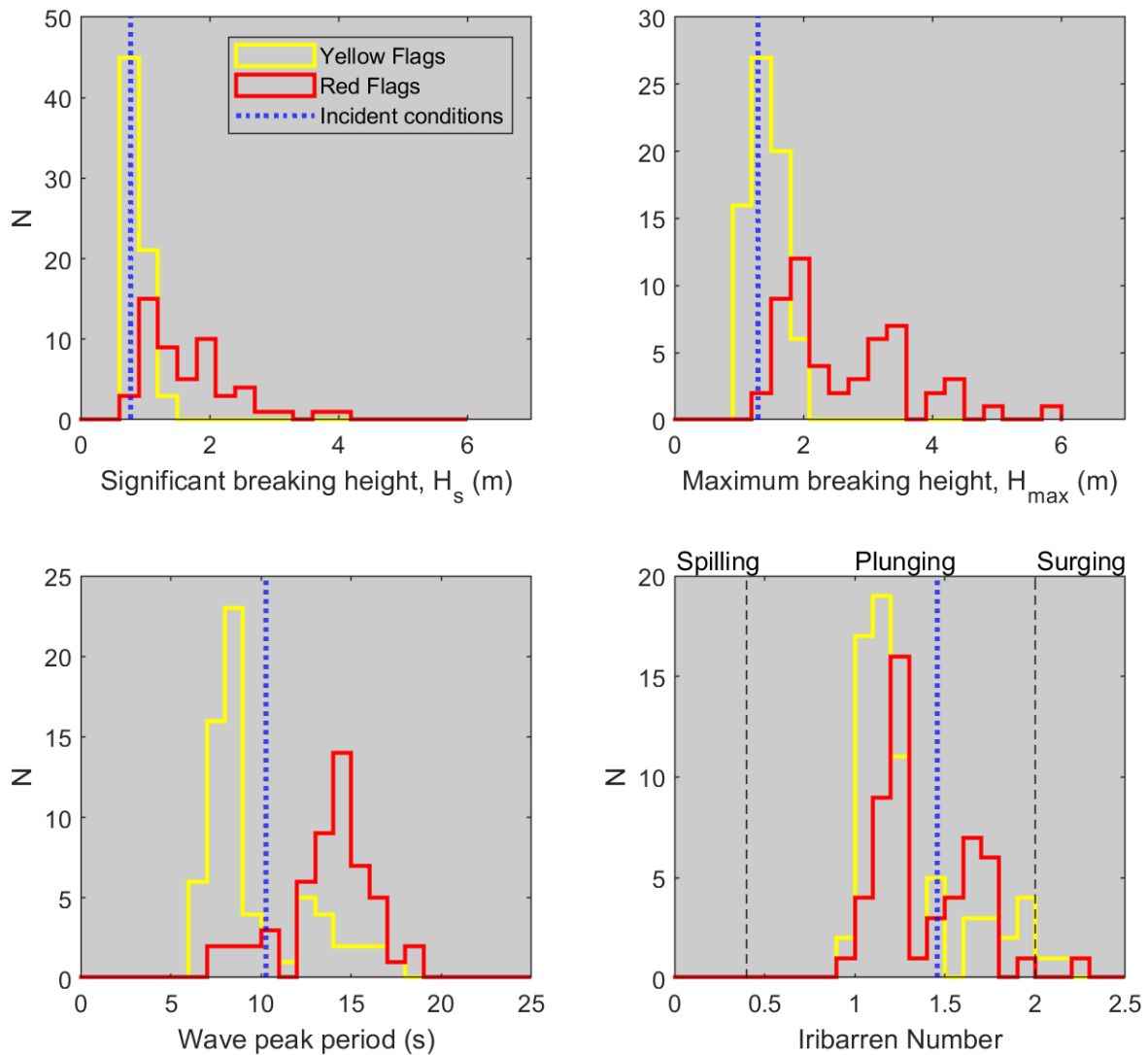


Figure 5-2. Histograms showing the distribution of wave conditions associated with each lifeguard hazard flag in March and April of 2018. The red and yellow lines in each panel show the distribution of wave conditions associated with the red and yellow flags in March and April of 2018, respectively. The red and yellow dashed lines show the average (median) condition associated with the red and yellow flags in March and April of 2018, respectively. The blue dotted line in each panel shows the wave conditions at the time of the bathing incident on 31st of March 2018. The y axis ('N') shows the number of half-day periods where each flag was flown during the

6. Conclusions

- Through a process of expert judgement using a combination of wave analysis, and assessment of in-situ and satellite imagery, the beach at Riu Funana beach is expected to sit within the ‘reflective’ or ‘low tide terrace’ end of the beach morphology spectrum. The likely beach profile gradient in the area of wave breaking is expected to be 0.1 (slope of 1-in-10), which represents a steep beach profile.
- Given the morphology type and steep gradient, shore-break impact injuries are expected to be the primary beach hazard type at Riu Funana beach.
- From processed wave model data, significant breaking wave heights at the site are predicted to vary from 0.3 – 4.4 m, but only exceed 1.4 m 10% of the time.
- Maximum breaking wave heights at the site are predicted to vary from 0.5 – 7.0 m, but only exceed 2.3 m 10% of the time.
- Wave conditions vary throughout the year, with average summer and winter significant breaking wave heights of 0.7 and 1.0 m, respectively, with maximum breaking wave heights of 1.2 and 1.7 m, respectively, and with peak wave periods of 8.8 and 11.5 s, respectively.
- Based on the significant wave height values, wave breaking is predicted to be predominantly within the ‘plunging’ regime, but periods characterised by ‘collapsing’ and ‘surging’ breakers are evident. These represent the most powerful wave breaker types.
- In-situ photographs of waves breaking at Riu Funana beach confirm that waves typically break very close to the beach, and under larger waves ($H_b > 1$ m) break as plunging breakers with considerable breaking intensity and power at the shoreline.
- On the day of the bathing incident on the 31st March 2018, wave heights are predicted to have been the same as the average annual breaking wave height, but lower than the average seasonal breaking wave height for the season in which the incident occurred (winter). Significant breaking wave height (H_b) at the time of the incident is estimated to have been 0.8 m (annual and seasonal averages = 0.9 and 1.0 m, respectively) and maximum breaking wave height (H_{bmax}) at the time of the incident is estimated to have been 1.3 m (annual and seasonal averages = 1.5 and 1.7 m, respectively).
- Accounting for uncertainties in the wave conditions and beach slope, there is 95% confidence that the breaker type was plunging, collapsing, or surging on the day of the incident, with the largest individual wave on the day predicted to have been either plunging or collapsing as it broke.
- The bathing incident occurred during relatively modestly sized breakers typical of other wave conditions associated with yellow lifeguard flags at the beach during March and April 2018. However, the combination of wave height and period (that contribute to the overall power of

the waves) sits within the transitional range representing the overlap between wave conditions typically associated with red and yellow flags in that period.

- The overlap in wave conditions associated with red and yellow flags during March and April of 2018 consists of 34 flag periods of the 122 in the log (28%) when significant wave height was between 0.8 and 1.3 m, and peak wave period was greater than 10 s, representing quite powerful breaking waves.

References

- Battjes, J. A. 1974. *Surf similarity*. 14th International Conference on Coastal Engineering. Copenhagen.
- Bujan, N., Cox, R. and Masselink, G. 2019. From fine sand to boulders: Examining the relationship between beach-face slope and sediment size. *Marine Geology*, **417**, 106012.
- Castelle, B., Scott, T., Brander, R., McCarroll, J., Robinet, A., Tellier, E., Korte, E. d., Simonnet, B. and Salmi, L.-R. 2019. Environmental controls on surf zone injuries on high-energy beaches. *Natural Hazards and Earth System Sciences*, **19**, (10), 2183-2205.
- Castelle, B., Scott, T., Brander, R. W. and McCarroll, R. J. 2016. Rip current types, circulation and hazard. *Earth-Science Reviews*, **163**, 1-21.
- Iribarren, C. and Nogales, C. 1949. Protection des Ports. XVIIth International Navigation Congress. Section II, Communication. **44**)
- Longuet-Higgins, M. S. 1952. On the statistical distribution of the height of sea waves. *Journal of Marine Research*, **11**, (3), 245-266.
- Masselink, G. and Short, A. D. 1993. The effect of tide range on beach morphodynamics and morphology: a conceptual beach model. *Journal of Coastal Research*, **9**, 785-800.
- Thornton, E. B. and Guza, R. T. 1983. Transformation of wave height distribution. *Journal of Geophysical Research: Oceans (1978–2012)*, **88**, 5925-5938.
- Van Rijn, L. C. 1993. *Principles of sediment transport in rivers, estuaries and coastal seas*. Aqua publications Amsterdam.
- van Rijn, L. C. 2014. A simple general expression for longshore transport of sand, gravel and shingle. *Coastal Engineering*, **90**, 23-39.
- Wright, L., May, S., Short, A. and Green, M. 1985. Beach and surf zone equilibria and response times. In: *Coastal Engineering 1984*. pp 2150-2164.
- Wright, L. D. and Short, A. D. 1984. Morphodynamic variability of surf zones and beaches: A synthesis. *Marine Geology*, **56**, 93-118.

Appendix A. Expertise of the CMAR team.

CMAR is the commercial consultancy arm of the Coastal Processes Research Group (CPRG) at the University of Plymouth, UK. Over the last 10 years, CPRG's research and consultancy work has significantly impacted beach lifeguarding risk assessment, training and policy in the UK, South Africa and New Zealand. CPRG's rip current forecasts are used in the UK and NZ, informing daily lifeguard resourcing. CPRG's expertise informed coroners' drowning inquiries in the UK and SA, and directly led to changes in risk management policy at two UK beaches and one beach in SA. The research underpins annual RNLI risk assessments at all UK bathing waters and annual lifeguard training material, and has informed rip current safety advice globally.

The team assembled for this project consist of **Professor Gerd Masselink** (director of CMAR), **Dr Tim Scott** (project lead), and **Dr Christopher Stokes** (lead consultant). **Gerd Masselink** is a Professor in Coastal Geomorphology with over 20 years' experience in collecting and analysing coastal data, and over 100 papers published in peer-reviewed international journals. Prof. Masselink published one of the most widely used beach morphology classification models and is an international expert on beach morphodynamics. **Dr Tim Scott** is a lecturer in Ocean Exploration and has been actively contributing to internationally recognised research in fields of beach and submarine geomorphology, rip current dynamics and coastal hazards. He has undertaken doctoral and post-doctoral research projects into physical beach hazards, and is an international expert on beach morphology, rip current dynamics, and physical beach hazards. **Dr Christopher Stokes** is a senior research consultant and has undertaken three consultancy projects for the RNLI mapping out which beaches in the UK pose the greatest life-risk to bathers, and has published research on modelling beach-user numbers and beach life-risk.

The team have collectively undertaken the following research and consultancy projects related to beach hazards:

- 2020–present, Newton Fund: Weather and Climate Science Services Partnership (WCSSP) SA: Marine and Coastal Applications. C Stokes: research consultant; T Scott: co-investigator; G Masselink: project lead. £80,000.
- 2018–2019, Auckland Council/Surf Life Saving Northern Regions: Safeswim Beach Risk Forecasting. C Stokes: research consultant; T Scott: co-investigator; G Masselink: project lead. £76,000.
- 2015–2018, RNLI: Quantification of Beach Risk in the UK and Northern Ireland. C Stokes: research consultant; T Scott: co-investigator; G Masselink: project lead. £105,000.

- 2012–2014, RNLI/MetOffice/Marine Institute: Topographic rip currents TOPORIP. T Scott: co-investigator. £99,000.
- 2010–2014, NERC/RNLI – Partnership grant: Dynamics of Rips and Implications for Beach Safety. T Scott: research fellow; G. Masselink: primary investigator. £550,000.
- 2009, RNLI: UK beach and hazards database project: Good Beach Guide integration. T Scott: primary investigator. £10,000.
- 2006–2008, RNLI: Classification and risk assessment of UK beaches. G Masselink: co-investigator. £30,000.

Below is a sample of some of the relevant research articles that the team have published in leading international peer-reviewed science journals:

- Castelle B, **Scott T**, Brander R, McCarroll RJ, Tellier E, de Korte E, Tackuy L, Robinet A, Simonnet B & Salmi L-R 2020 'Wave and Tide Controls on Rip Current Activity and Drowning Incidents in Southwest France' *Journal of Coastal Research* 95, (sp1) 769-769.
- Castelle B, **Scott T**, Brander R, McCarroll J, Robinet A, Tellier E, de Korte E, Simonnet B & Salmi L-R 2019 'Environmental controls on surf zone injuries on high-energy beaches' *Natural Hazards and Earth System Sciences* 19, (10) 2183-2205.
- **Scott T**, Castelle B, Almar R, Senechal N, Floc'h F & Detandt G 2018 'Controls on Flash Rip Current Hazard on Low-Tide Terraced Tropical Beaches in West Africa' *Journal of Coastal Research* 92-99.
- Castelle B, Brander R, Tellier E, Simonnet B, **Scott T**, McCarroll J, Campagne J-M, Cavailhes T & Lechevrel P 2018 'Surf zone hazards and injuries on beaches in SW France' *Natural Hazards*.
- **Stokes, C., Masselink, G., Revie, M., Scott, T., Purves, D. and Walters, T., 2017.** Application of multiple linear regression and Bayesian belief network approaches to model life risk to beach users in the UK. *Ocean & Coastal Management*, 139, pp.12-23.
- Castelle B, **Scott T**, Brander RW & McCarroll RJ 2016 'Rip current types, circulation and hazard' *Earth-Science Reviews* 163, 1-21
- **Scott T**, Austin M, **Masselink G** & Russell P 2016 'Dynamics of rip currents associated with groynes — field measurements, modelling and implications for beach safety' *Coastal Engineering* 107, 53-69.
- **Scott T, Masselink G**, Austin MJ & Russell P 2014 'Controls on macrotidal rip current circulation and hazard' *GEOMORPHOLOGY* 214, 198-215
- Austin MJ, **Masselink G, Scott TM** & Russell PE 2014 'Water-level controls on macro-tidal rip currents' *Continental Shelf Research* 75, 28-40.

- Austin, M.J., **Scott, T.M.**, Russell, P.E. and **Masselink, G.**, 2013. Rip current prediction: development, validation, and evaluation of an operational tool. *Journal of coastal research*, 29(2), pp.283-300.
- **Scott T, Masselink G** & Russell P 2011 'Morphodynamic characteristics and classification of beaches in England and Wales' *MARINE GEOLOGY* 286, (1-4) 1-20.
- Austin M, **Scott T**, Brown J, Brown J, MacMahan J, **Masselink G** & Russell P 2010 'Temporal observations of rip current circulation on a macro-tidal beach' *Continental Shelf Research* 30, (9) 1149-1165.
- **Scott T**, Russell P, **Masselink G**, Wooler A & Short A 2007 'Beach Rescue Statistics and their Relation to Nearshore Morphology and Hazards: A Case Study for Southwest England' *J COASTAL RES (SI 50)* 1-6.
- **Masselink G** & Short A 1993 'The effect of tide range on beach morphodynamics and morphology - a conceptual beach model' *Journal of Coastal Research* 9, (3) 785-800.

Appendix B. Processing of wave model data.

The offshore wave model data provides significant wave height, but does not provide predictions of maximum wave height. For this report, maximum wave height has been derived from significant wave height using a well-established statistical relationship based on the observation that the distribution of wave heights in the ocean usually follows a Rayleigh distribution (Longuet-Higgins, 1952; Thornton and Guza, 1983):

$$H_{max} = 0.707 H_s \sqrt{\ln J} \quad (1)$$

Where H_s = the offshore significant wave height output by the wave model, and J = the number of waves in the random sea over a given period of time. J can be estimated as $J = \Delta t / T_p$, where Δt is the time period of interest, here applied using the temporal resolution of the wave model (3 hrs = 10800 s) and T_p is the mean wave period. \ln is the normal logarithm.

Breaking wave height at the beach for both significant wave heights and maximum wave heights was calculated using an empirical equation (van Rijn, 2014) that estimates breaking wave height, water depth and direction using linear wave theory and Snell's law for refraction:

$$h_b = [(H^2 C_o \cos \theta_o) / (1.8 \gamma^2 g^{0.5})]^{0.4} \quad (2)$$

and

$$\sin \theta_b = (C_b / C_o) \sin \theta_o \quad (3)$$

where h_b = the water depth at the point of wave breaking, H = the offshore wave height output by the wave model (this can either be significant or maximum wave height, depending on which parameter is being shoaled to breaking height), C_o , C_b = the offshore and breaking wave propagation speeds, and θ_o , θ_b = the offshore and breaking wave incidence angles relative to shore normal (for Riu Funana beach, shore normal = 275°). Snell's law for refraction is limited to waves arriving from a direction within +/- 90° of shore-normal, and therefore all waves were assumed to arrive at Riu Funana beach within this directional window. C_o was calculated from the deepwater wavelength, L_o , and peak wave period, T_p , as $C_o = L_o / T_p$, while C_b was calculated as $C_b = \sqrt{g h_b}$. Breaker criterion γ is a key

parameter that determines the depth at which wave breaking occurs, and was set using the widely applied value of 0.78 (Munk, 1949).

The breaking wave height can then be calculated as the product of the breaker criterion and breaker depth:

$$H_b = \gamma h_b \quad (4)$$

The Iribarren Number was calculated from the **maximum** breaking wave height, deepwater wavelength and estimated beach slope ($\tan \beta$) as (Battjes, 1974):

$$\varepsilon = \frac{\tan \beta}{\sqrt{H_b/L_0}} \quad (5)$$

Appendix C. Breaker type distributions

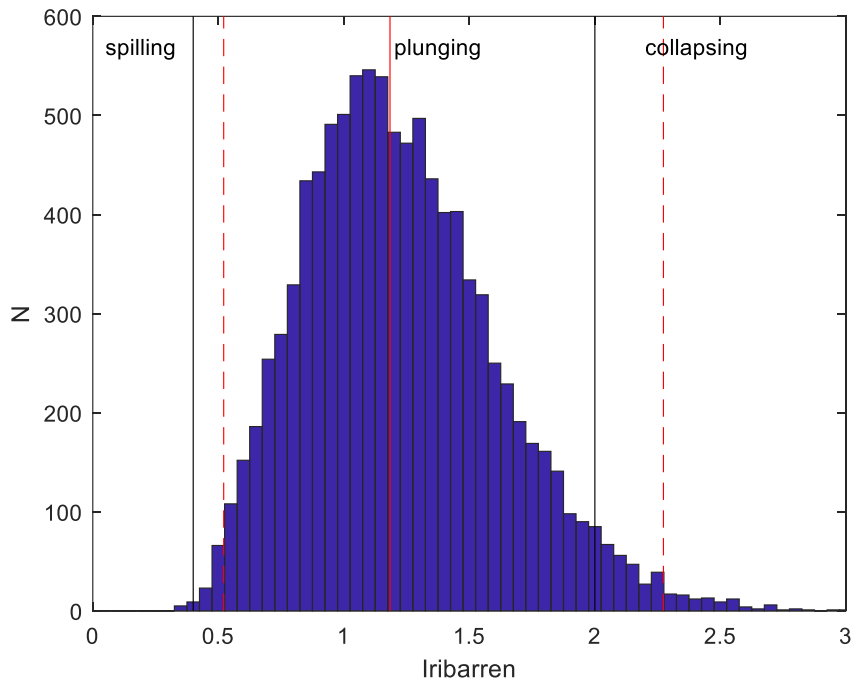


Figure C-1. Distribution of Iribarren number values from a monte-carlo assessment of breaker type (described in Section 4), using the maximum breaking wave height (H_{max}) to determine the Iribarren number. The red line shows the median Iribarren number, while the red dotted lines show the lower and upper 95% confidence bounds. The black lines show the thresholds for the spilling, plunging, and surging breaker types (collapsing breakers occur at the threshold between plunging and surging breakers).

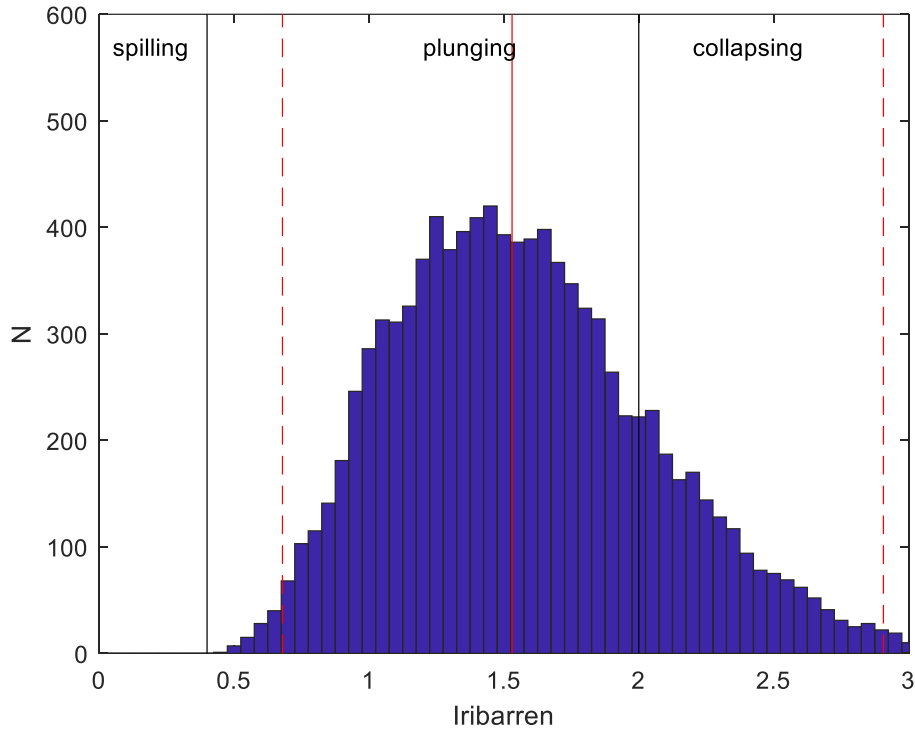


Figure C-2. Distribution of Iribarren number values from a monte-carlo assessment of breaker type (described in Section 4), using the significant breaking wave height (H_s) to determine the Iribarren number. The red line shows the median Iribarren number, while the red dotted lines show the lower and upper 95% confidence bounds. The black lines show the thresholds for the spilling, plunging, and surging breaker types (collapsing breakers occur at the threshold between plunging and surging breakers).

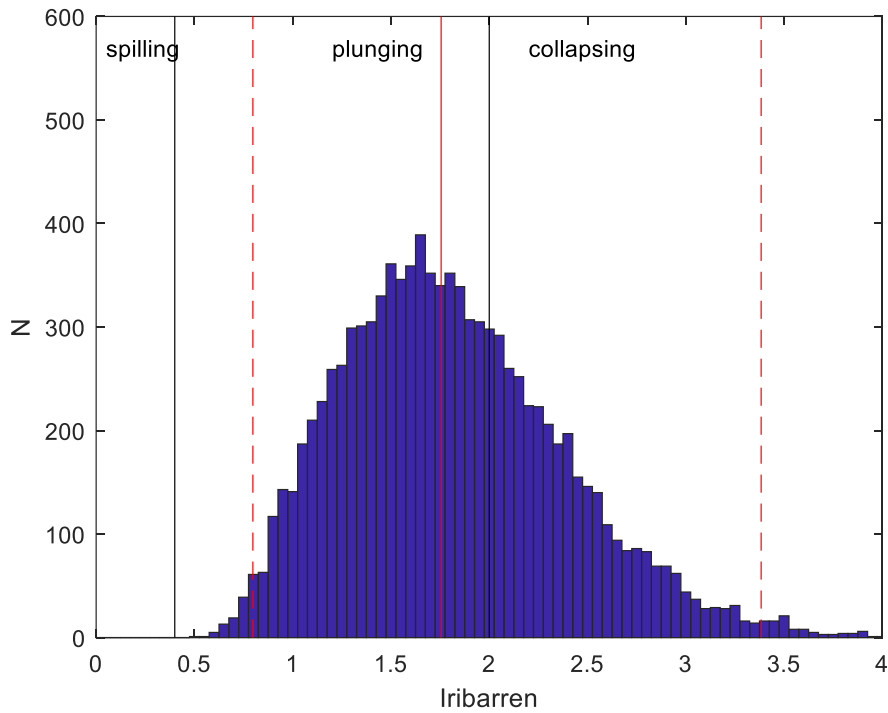


Figure C-3. Distribution of Iribarren number values from a monte-carlo assessment of breaker type (described in Section 4), using the root-mean-square average breaking wave height (H_{rms}) to determine the Iribarren number. The red line shows the median Iribarren number, while the red dotted lines show the lower and upper 95% confidence bounds. The black lines show the thresholds for the spilling, plunging, and surging breaker types (collapsing breakers occur at the threshold between plunging and surging breakers).